Chinese Chemical Letters 35 (2024) 108461

Contents lists available at ScienceDirect

Chinese Chemical Letters

journal homepage: www.elsevier.com/locate/cclet

S1-supported Pd@CeO_2 *quasi*-core@shell materials as advanced catalysts for selective hydrogenation of furfural

Xiang Chu[a,b,1], Lingling Zhang[a,1], Ke Wang[a,b], Rui Zhang[a,b], Xiao Wang[a,b,*], Shuyan Song[a,b,*], Hongjie Zhang[a,b,*]

[a] State Key Laboratory of Rare Earth Resource Utilization, Changchun Institute of Applied Chemistry, Chinese Academy of Sciences, Changchun 130022, China
[b] School of Applied Chemistry and Engineering, University of Science and Technology of China, Hefei 230026, China

ARTICLE INFO

Article history:
Received 6 January 2023
Revised 23 March 2023
Accepted 14 April 2023
Available online 16 April 2023

Keywords:
Core@shell
Palladium
Ceria
Auto-redox synthesis
Hydrogenation

ABSTRACT

Bare Pd metal nanoparticles invariably suffer from poor selectivity in furfural hydrogenation by forming flat configurations, with the aromatic ring of the substrate molecules parallel to the metal surface. Herein, we put forward a promising solution by using CeO_2 as promoters to modify Pd nanoparticles for modulating the adsorption behaviors of furfural molecules. To achieve the highly-desired ultra-small Pd@CeO_2 core@shell nanostructure, a "constrained auto-redox" synthesis is developed, in which silicalite-1 supports play the key role of providing their surface as the landing place of PdO_x precursors for inhibiting the overgrowth and the deformation. To the best of our knowledge, this is one of the smallest core@shell materials obtained from aqueous synthesis. When evaluated as catalysts, Pd@CeO_2/S-1 gives 98.9% conversion of furfural with 94.3% selectivity for furfural alcohol in 15 h, which is much better than that of Pd/S-1 (88.6% conversion with 44.3% selectively). The DFT simulation reveals a strong interaction between the defects of CeO_2 and the oxygen atom of the –CHO group in furfural molecules, which benefits the selective hydrogenation occurred in the –CHO group rather than the furan ring.

Selective hydrogenation of renewable biomass to highly value-added biofuels and fine chemicals has attracted significant research interest owing to mankind's earnest efforts to reduce their dependence on fossil resources [1–4]. Noble metals are widely applied for triggering this catalysis because of the active sites on them and their capability to dissociate H_2 under mild conditions [5–7]. Generally, the catalytic performance is highly dependent on the intrinsic properties of the catalyst, coordination environments of the surface atoms, and their interactions with supports. A single-component noble metal without proper surface modification invariably exhibits inadequate selectivity, resulting in high yields of undesirable byproducts [8–10]. A primary reason for this poor selectivity is the favorable formation of a flat configuration, with the aromatic rings of the substrate molecules parallel to the metal surface [11–13]. To overcome this drawback, several promising strategies have been proposed, which include manipulation of the surface charge parameters and modulation of the surrounding space-confined effect by processes such as overcoating noble metals with special organic ligands [14], decreasing the particle size of noble metals from the nanometer to atomic scale [15,16], coupling multiple components together in the form of alloys or core@shell nanostructures [17–19], and encapsulating noble metal species within zeolites or metal-organic frameworks [20–23]. All these approaches for improving the performance of noble metal catalysts involve the common principle of manipulating the adsorption geometry of the substrate molecules. Despite the development of such strategies, rationalization of the surface state of noble metals for a particular catalytic process is still a pressing challenge.

Recently, transition metal oxides have shown significant potential as promoters for noble metal catalysts in selective hydrogenation reactions [10,24,25]. The hybrid material obtained by loading transition metal oxide species on the surface of a target noble metal exhibits remarkably enhanced catalytic performance. Promotion of the catalytic activity can be attributed to the oxophilic character of the transition metal cations, which can effectively prevent the formation of a flat configuration. For instance, Zheng and coworkers successfully demonstrated that the catalytic selectivity of Pt nanoparticles (NPs) could be significantly promoted by coupling with $Fe(OH)_x$ clusters [10]. The corresponding density func-

* Corresponding authors at: State Key Laboratory of Rare Earth Resource Utilization, Changchun Institute of Applied Chemistry, Chinese Academy of Sciences, Changchun 130022, China.
E-mail addresses: wangxiao@ciac.ac.cn (X. Wang), songsy@ciac.ac.cn (S. Song), hongjie@ciac.ac.cn (H. Zhang).
[1] These authors contributed equally to this work.

https://doi.org/10.1016/j.cclet.2023.108461
1001-8417/

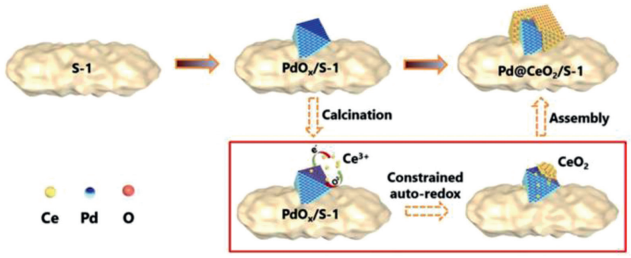

Fig. 1. Schematic illustration of the formation process of S-1 supported Pd@CeO_2 core@shell materials.

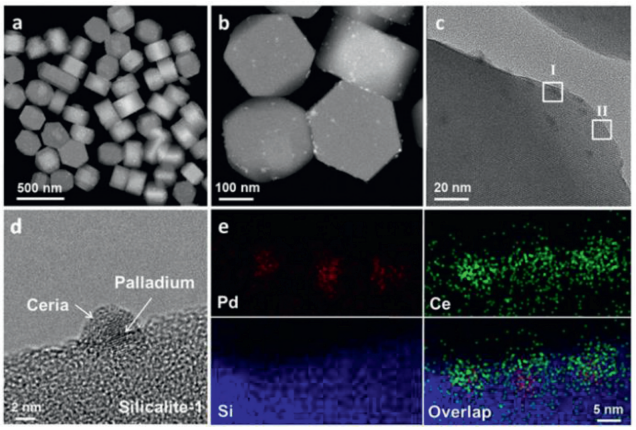

Fig. 2. (a, b) HAADF-STEM, (c, d) TEM and (e) element mapping images of S-1 supported Pd@CeO_2 core@shell materials.

tional theory (DFT) calculation revealed that 3-nitrostyrene preferred to bind at the Fe(OH)$_x$-Pt interface through the –NO_2 group rather than the -C=C group, thereby suppressing indiscriminate hydrogenation efficiently. A similar effect was observed by Xiao *et al*. for the Sn-Pt-TiO_2 system [24]. Furthermore, Qin and coworkers successfully tailored the reaction pathway for nitroaromatic hydrogenation over TiO_2-supported Au NPs by atomic deposition of NiO species [25]. They found that the adsorption of azoxybenzene on the NiO-modified Au surface was stronger than that on bare Au surface, resulting in a seismic shift in the catalytic selectivity. These transition metal oxides are very stable, highly abundant, and easily available, thereby increasing the possibilities of their use in practical applications. However, only a few strategies involving the combination of transition metal oxide and noble metal to promote the catalytic performance has been successful so far. Therefore, two aspects are central to the success of such strategies: rational selection of transition metal oxides as promoters and development of feasible routes for material synthesis.

In this study, we focused on Pd, which is a widely used active component in selective hydrogenation but has poor selectivity [26–28]. CeO_2 supports have high thermal stability and abundant surface defects and have been used as catalyst promoters; moreover, they involve in strong interactions with various noble metals [29,30]. A "constrained auto-redox strategy" is developed for the *in situ* construction of ultrasmall Pd@CeO_2 core@shell materials supported by silicalite-1 (S-1). S-1 plays a crucial role in trapping oxidative PdO_x species acting as the precursors to react with reductive Ce^{3+} species, thereby restricting its overgrowth and aggregation (Fig. 1). Compared to the unmodified Pd/S-1 sample, the prepared core@shell material exhibited significant improvement in the catalytic performance for the selective hydrogenation of furfural. The densely coated CeO_2 shell is considered to be the primary reacting surface, which blocked the direct contact of Pd surface with furfural molecules, thus inhibiting the formation of the flat configuration of furfural molecules. DFT calculations revealed that furfural was preferably adsorbed on the defect sites of CeO_2 NPs through the -CHO group rather than the furan ring, owing to the relatively high adsorption energy, leading to the enhancement of FA selectivity.

S-1 particles were synthesized hydrothermally using a previously reported method [31,32]. Transmission electron microscopy (TEM) images (Fig. S1 in Supporting information) revealed that the product, with an average particle size of ~280 nm, is highly uniform and monodispersed. The corresponding X-ray diffraction (XRD) pattern verifies its MFI-type structure (Fig. S2 in Supporting information). Subsequently, Na_2PdCl_4 and hexamethylenetetramine (HMT) were added to an aqueous dispersion containing S-1 crystals, followed by heating at 80 °C to generate ultrasmall Pd species. After that, the obtained precursor was calcinated at 300 °C in air for 1 h to obtain PdO_x/S-1. TEM images (Fig. S3 in Supporting information) revealed the formation of small NPs dispersed homogeneously on the surface of S-1, and average particle size of PdO_x nanoparticles are 2.17 nm on average.

Next, an auto-redox synthesis was conducted *via* the reaction of PdO_x/S-1 with an aqueous solution of cerium acetate ($Ce(Ac)_3$). High-angle annular dark-field scanning transmission electron microscopy was used to investigate the fine structure of the product. Figs. 2a and b show that the hexagonal morphology of S-1 was well preserved; small particles on the surface of S-1 could be easily distinguished upon closer observation. The newly generated particles exhibited a similar degree of dispersion (26.84% for Pd) but much larger particle sizes (~6.8 nm on average) compared to the initial PdO_x species. To the best of our knowledge, this is one of the smallest core@shell materials obtained from aqueous synthesis. Composition of these loaded particles was examined by energy dispersive X-ray spectroscopy (EDX). As marked in Fig. 2c, two different areas, a small particle (area I) and its neighboring black area (area II), were selected as the target for investigation, and it was revealed that both Ce and Pd exist only in the small particles (Figs. S4 and S5 in Supporting information). This confirms the successful *in situ* surface deposition. Furthermore, high-resolution transmission electron microscopy image (Fig. 2d) revealed a core@shell hybrid nanostructure of the product (Fig. 2d), which was coincident with the elemental mapping analysis (Fig. 2e) homogeneous distribution of Pd at the center, with Ce present only in the outer region. Crystallinity of the product was investigated by XRD (Fig. S6 in Supporting information). The peaks corresponding to Pd or CeO_2 were masked by those of S-1. This could be attributed to the relatively low CeO_2 and Pd contents and the higher crystallinity of S-1. Inductively coupled plasma-mass spectrometry also confirmed the co-existence of Ce and Pd in the Pd@CeO_2/S-1 sample. The Pd and CeO_2 contents were 0.12 and 0.93 wt%, respectively.

To verify the mechanism of the redox reaction, changes in the valence states of Pd before and after the auto-redox reaction were analyzed by X-ray photoelectron spectroscopy (XPS, Fig. S7 in Supporting information). Deconvolution of the XPS curves revealed that the Pd^0/Pd^{2+} molar ratios were 0.92 and 3.33 in the PdO_x/S-1 and Pd@CeO_2/S-1 samples, respectively, suggesting a successful redox reaction between the PdO_x and Ce^{3+} species. Furthermore, the peaks corresponding to Pd^0 $3d_{3/2}$ and $3d_{5/2}$ in Pd@CeO_2/S-1 show an apparent positive shift with respect to that of PdO_x/S-1, which indicates the occurrence of electron transfers from Pd to CeO_2 [6,33,34]. The XPS spectrum of Ce in Pd@CeO_2/S-1 (Fig. S8 in Supporting information) is consistent with that of standard CeO_2 samples, serving as direct evidence for the formation of crystalline CeO_2 NPs [33,34]. In addition, a control experiment was conducted in which bare S-1 crystals, instead of PdO_x/S-1, were reacted with

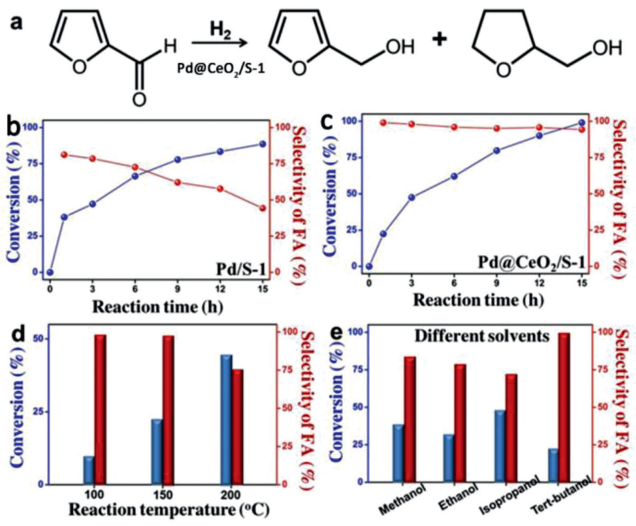

Fig. 3. (a) Schematic illustration of furfural hydrogenation. The conversion of furfural and selectivity to FA *versus* the reaction time over (b) Pd@CeO_2/S-1 and (c) Pd/S-1. The investigation of (d) reaction temperature and (e) solvent effects for the catalytic performance of Pd@CeO_2/S-1 catalyst. Reaction conditions: 10 mg of catalyst, 10 μL of furfural, and 10 mL of the solvent; temperature 423.15 K, pressure 2 MPa.

$Ce(Ac)_3$, keeping the same Ce concentration of Pd@CeO_2/S-1 (0.9 wt% for Ce). Although small particles were generated, no assembled structures were observed on the surface of S-1 (Fig. S9 in Supporting information). In another control experiment, $Ce(Ac)_3$ was replaced by $(NH_4)_4Ce(SO_4)_4$. The corresponding TEM images and EDX spectrum (Fig. S10 in Supporting information) clearly indicate the existence of independent CeO_2 NPs. These results establish the crucial role of PdO_x, which provides active sites for triggering the *in situ* deposition of the CeO_2 layer. Therefore, the overall auto-redox process can be completed in two steps. Initially, reductive CeO_x species are generated in the reaction medium owing to the hydrolysis of $Ce(Ac)_3$. Consequently, the redox reaction is induced, triggering the conversion of PdO_x to metallic Pd and the selective deposition of CeO_2 NPs for the formation of the final core@shell nanostructure.

An accelerated aging test was performed according to previous reports to investigate the stability of the obtained core@shell materials [35–37]. The samples were first calcinated at 650 °C in air for 5 h and then reduced at 200 °C in H_2/Ar atmosphere for 2 h. TEM images (Figs. S11a–g in Supporting information) captured after three successful cycles show well-distributed uniform Pd@CeO_2 NPs on the surface of S-1, with slight increase in the average particle size from 6.8 nm to 8.2 nm. No obvious aggregation and migration occurred, suggesting ultra-high stability. This was in contrast to Pd/S-1, which exhibited poor stability. Accompanied by the cycling performance, much larger particles with larger size distributions were observed in the corresponding TEM images (Figs. S11i–p in Supporting information). The average particle size increased from 3.5 nm to 7.9, 9.1 and 10.8 nm after the first, second, and third cycles, respectively. This clearly illustrates that the core@shell structure can effectively protect the Pd core from high-temperature sintering.

The catalytic properties of Pd@CeO_2/S-1 and Pd/S-1 were examined in the selective hydrogenation of furfural as a model reaction (Fig. 3a). Prior to experiments, both the samples were activated at 300 °C in an H_2/Ar atmosphere for 2 h. It is evident from Fig. 3b that the catalytic activity of Pd/S-1 was relatively high in the first hour, and 38.1% of furfural could be converted to furfural alcohol (FA) with 81.2% yield. However, it loses its activity rapidly, and the furfural conversion remained constant at 88.6% after 15 h. This can be attributed to the damage of the Pd surface and the formation of coke [38]. Moreover, gas chromatography–mass spectrometry (GC–MS) revealed the occurrence of many side reactions along with the main reaction. The final product contained 32.4% of tetrahydrofuran alcohol (THFA) derived from over-hydrogenation and 9.8% of C10 products generated through condensation. In contrast, with a thin CeO_2 layer overcoated over Pd, the initial reaction rate decreased, and 22.4% of furfural was converted in the first hour (Fig. 3c). The lower initial activity can be attributed to the poor diffusion due to the formation of a core@shell structure. However, the first-hour activity was well retained during the rest of the reaction time: 98.9% conversion of furfural was achieved after 15 h. More importantly, the selectivity for FA was significantly improved to 94.3% in final product, indicating that the core@shell structure could efficiently prevent the deactivation as well as the side reactions. The reaction kinetics investigations demonstrate the higher activity of Pd@CeO_2/S-1 than that of Pd/S-1 (Fig. S12 in Supporting information). Benefiting from the unique *quasi*-core@shell structure, our catalysts exhibit comparable catalytic activity and selectivity, compared with state-of-art furfural hydrogenation% catalysts (Table S1 in Supporting information).

We further investigated the effects of temperature, solvent, and CeO_2 shell thickness on the catalytic performance of Pd@CeO_2/S-1. Fig. 3d shows that the extent of conversion in the first hour changed from 22.4% to 9.7% and 44.5% upon changing the reaction temperature from 150 °C to 100 and 200 °C, respectively. This is in agreement with previous reports, which state that the reaction rate increases with increasing temperature [39,40]. However, a higher temperature also increases the probability of side reactions, and only 75.7% of furfural was converted into FA at 200 °C. Therefore, we conducted the catalysis at 150 °C to achieve a balance between the activity and selectivity. Additionally, it was found that the catalytic activity of Pd@CeO_2/S-1 was highly sensitive to solvents. Fig. 3e shows that the conversion in the first hour increased to 37.6%, 31.3% and 47.0% in methanol, ethanol, and isopropanol, respectively, meanwhile, the catalytic selectivity for FA was deceased in all these solvents. This can be attributed to the varying ionic strengths of the solvents [3,39]. It has been reported that the increase in solvent molecules' polar strength would promote the adsorption and activation processes of hydrophilic C=O bonds, leading to the enhancement of hydrogenation activity [41,42]. However, at the same time, the corresponding GC results demonstrate that it is easy to occur the condensation reaction between short-chain alcohols and furfural molecules. Next, We further synthesized a series of Pd@CeO_2/S-1 catalysts with different CeO_2 contents by changing the feeding amount of $Ce(Ac)_3$. As shown in Fig. S14 (Supporting information), when doubling the $Ce(Ac)_3$ feeding amount (Pd@CeO_2–H/S-1), the furfural conversion is decreased to 15.43% in the first hour, but the selectivity is well maintained. The phenomenon might be induced by the diffusion problem caused by increasing the CeO_2 shell thickness. In contrast, when halving the $Ce(Ac)_3$ feeding amount (Pd@CeO_2-L/S-1), though the furfural conversion is increased to 30.1% in the first hour, only 90% of FA is obtained. The phenomenon might be caused by the generation of incomplete core@shell structure in this condition, which may increase the chances of contact between Pd surface and furfural molecules, thus contributing to the decreased selectivity. Finally, the cycling performance test of Pd@CeO_2 was carried out by monitoring the changes in the conversion and selectivity (Fig. S15 in Supporting information). After five successful cycles, over 90.7% conversion of furfural with 92.2% yield of FA was obtained, and there is no obvious change in TEM images for fresh Pd and after cycles test (Fig. S16 in Supporting information), suggesting the robustness of such core@shell catalysts.

Subsequently, DFT calculations were performed to determine the model of furfural adsorption on various catalysts and to fur-

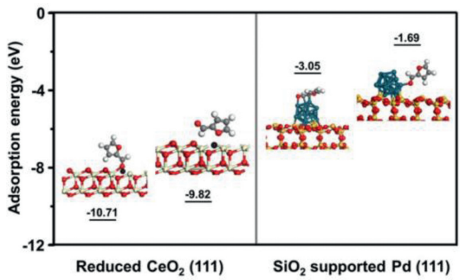

Fig. 4. Summary of adsorption models of furfural on reduced CeO_2 (111) face and SiO_2 supported Pd_{13}.

ther verify the positive contribution of the CeO_2 shell in performance enhancement. Initially, a computational model composed of a small Pd cluster (Pd_{13}) loading on a SiO_2 support was established to save computational resources. Furfural contains two functional groups that interact strongly with the Pd surface atoms: the –CHO group and the furan ring. When furfural is adsorbed on Pd_{13} *via* the furan ring, a flat configuration is adopted (Fig. 4). The adsorption energy in this case was calculated as –3.05 eV, which is much higher than that when furfural bonds with Pd through the O atom in the –CHO group (–1.69 eV). This suggests that furfural is preferably adsorbed *via* the furan ring; this is also consistent with previous reports and is considered to be the main reason for the poor catalytic selectivity of Pd NPs [43,44]. Next, we studied the adsorption of furfural on reduced-CeO_2 surface. The surface defects are simulated as the active sites by referring to the previous reports (CeO_2 has a high concentration of surface oxygen vacancy) and considering our experimental conditions (the catalysts were reduced at 300 °C in H_2/Ar atmosphere) [9,45]. Calculations reveal that furfural prefers to bond with the defect site *via* the O atom in the –CHO group (10.71 eV) rather than the O atom in the furan ring (9.82 eV). More importantly, DFT calculations predict that the flat configuration cannot exist, and this can be attributed to the ultrahigh oxophilicity of Ce cations. Therefore, promotion of the catalyst activity by CeO_2 shell can be mainly attributed to its strong interaction with the O atom in the –CHO group, which benefits the selective hydrogenation occurred in the –CHO group. Besides, for investing the role of Pd in hydrogenation, we conducted the H_2-TPR of Pd@CeO_2/S-1 and CeO_2/S-1 with the same Ce content (Fig. S17 in Supporting information). The strong reduction peaks between 350 °C and 500 °C could be ascribed to the reduction of surface-capping oxygen of ceria promoted by the hydrogen spillover effect from Pd atoms to the support. To further check the hydrogen spillover, we processed an H_2 treatment for the mixture of WO_3 with Pd@CeO_2/S-1 and CeO_2/S-1 under mild temperature, respectively. And only the Pd@CeO_2/S-1 gives a dark color of the tungsten species (Fig. S18 in Supporting information). Because the migrating activated H would reduce the WO_3 forming dark blue H_xWO_3. Thus, we infer that the Pd activates the H_2 and then the activated hydrogen species flow to the surface of CeO_2 attacking the -CHO group of adsorbed furfurals, generating the FA.

In summary, ultrasmall Pd@CeO_2 core@shell NPs were successfully synthesized through a clean and wet-chemistry route. Reactive PdO_x species were initially anchored on S-1 support to inhibit the overgrowth and deformation during the sequential conversion. Thereafter, they played a crucial role by providing active sites for inducing the *in situ* deposition of CeO_2 NPs. Owing to the unique structural features, the obtained Pd@CeO_2/S-1 sample exhibited significantly enhanced catalytic activity in furfural hydrogenation. It is speculated that the developed "confined auto-redox reaction" will pave a new way for designing and constructing complex core@shell materials that have applications in the field of catalysis.

Declaration of competing interest

The authors declare that they have no known competing financial interests or personal relationships that could have appeared to influence the work reported in this paper.

Acknowledgments

This work was supported by the financial aid from National Science and Technology Major Project of China (No. 2022YFB3504000) and National Natural Science Foundation of China (Nos. 22020102003, 22025506 and 22271274).

Supplementary materials

Supplementary material associated with this article can be found, in the online version, at doi:10.1016/j.cclet.2023.108461.

References

[1] X. Luo, Y. Li, N.K. Gupta, et al., Angew. Chem. Int. Ed. 59 (2020) 11704–11716.
[2] C. Xu, E. Paone, D. Rodríguez-Padrón, et al., Chem. Soc. Rev. 49 (2020) 4273–4306.
[3] H. Yu, Y. Xu, K. Havener, et al., Small 18 (2022) 2106893.
[4] C. Dong, Q. Yu, R.P. Ye, et al., Angew. Chem. Int. Ed. 59 (2020) 18374–18379.
[5] Z. Dou, Z. Zhang, H. Zhou, et al., Angew. Chem. Int. Ed. 60 (2021) 16399–16403.
[6] Y. Feng, W. Xu, B. Huang, et al., J. Am. Chem. Soc. 142 (2020) 962–972.
[7] S.M. Rogers, C.R.A. Catlow, C.E. Chan-Thaw, et al., ACS Catal. 7 (2017) 2266–2274.
[8] C. Xu, H. Wu, Z. Zhang, et al., Chem. Sci. 13 (2022) 1629–1635.
[9] S. Zhang, C.R. Chang, Z.Q. Huang, J. Am. Chem. Soc. 138 (2016) 2629–2637.
[10] Y. Wang, R. Qin, Y. Wang, et al., Angew. Chem. Int. Ed. 59 (2020) 12736–12740.
[11] Q. Liu, J. Wu, J. Kang, et al., Nanoscale 14 (2022) 15462–15467.
[12] W. Gong, C. Chen, H. Wang, et al., Chin. Chem. Lett. 29 (2018) 1617–1620.
[13] H. Du, X. Ma, M. Jiang, et al., Chin. Chem. Lett. 33 (2022) 912–915.
[14] S.H. Pang, C.A. Schoenbaum, D.K. Schwartz, et al., ACS Catal. 4 (2014) 3123–3131.
[15] M. Macino, A.J. Barnes, S.M. Althahban, et al., Nat. Catal. 2 (2019) 873–881.
[16] Y. Ling, H. Ge, J. Chen, et al., Adv. Sci. 9 (2022) 2202144.
[17] O.B. Ayodele, R. Cai, J. Wang, et al., ACS Catal. 10 (2020) 451–457.
[18] J. Liu, M.B. Uhlman, M.M. Montemore, et al., ACS Catal. 9 (2019) 8757–8765.
[19] T. Mitsudome, T. Urayama, K. Yamazaki, et al., ACS Cata. 6 (2016) 666–670.
[20] C. Wang, L. Wang, J. Zhang, et al., J. Am. Chem. Soc. 138 (2016) 7880–7883.
[21] H.J. Cho, D. Kim, B. Xu, ACS Catal. 10 (2020) 4770–4779.
[22] Y. Long, S. Song, J. Li, et al., ACS Catal. 8 (2018) 8506–8512.
[23] C. Bian, D. Li, Q. Liu, et al., Chin. Chem. Lett. 33 (2022) 1169–1179.
[24] L. Wang, E. Guan, J. Zhang, et al., Nat. Commun. 9 (2018) 1362.
[25] J.X. Zhao, C.Q. Chen, C.H. Xing, et al., ACS Catal. 10 (2020) 2837–2844.
[26] Y. Ma, H. Wang, G. Xu, et al., Chin. Chem. Lett. 28 (2017) 1153–1158.
[27] L. Zhang, H. Yu, H. Yu, et al., Chin. Chem. Lett. 25 (2014) 1132–1136.
[28] M. Guo, H. Li, Y. Ren, et al., ACS Catal. 8 (2018) 6476–6485.
[29] X. Wang, D. Liu, S. Song, et al., J. Am. Chem. Soc. 135 (2013) 15864–15872.
[30] X. Wang, Y. Zhang, S. Song, et al., Angew. Chem. Int. Ed. 55 (2016) 4542–4546.
[31] C.C. Hou, L. Zou, L. Sun, et al., Angew. Chem. Int. Ed. 59 (2020) 7384–7389.
[32] Q. Sun, N. Wang, Q. Bing, et al., Chem 3 (2017) 477–493.
[33] R.V. Gulyaev, A.I. Stadnichenko, E.M. Slavinskaya, et al., Appl. Catal. A: Gen. 439 (2012) 41–50.
[34] M. Mateen, M.N. Akhtar, L. Gao, et al., Nano Res. 15 (2022) 7107–7115.
[35] L. Liu, M. Lopez-Haro, C.W. Lopes, et al., Nat. Mater. 18 (2019) 866–873.
[36] L. Liu, U. Díaz, R. Arenal, et al., Nat. Mater. 16 (2017) 132–138.
[37] L. Wang, L. Wang, X. Meng, et al., Adv. Mater. 31 (2019) 1901905.
[38] M.S. Zanuttini, M. Gross, G. Marchetti, et al., Appl. Catal. A: Gen. 587 (2019) 117217.
[39] L. Chen, J. Ye, Y. Yang, et al., ACS Catal. 10 (2020) 7240–7249.
[40] T. Asano, H. Takagi, Y. Nakagawa, et al., Green Chem. 21 (2019) 6133–6145.
[41] X. Gao, S. Tian, Y. Jin, et al., ACS Sustain. Chem. Eng. 8 (2020) 12722–12730.
[42] P. Mäki-Arvela, L. Tiainen, A.K. Neyestanaki, et al., Appl. Catal. A: Gen. 237 (2002) 181–200.
[43] V. Vorotnikov, G. Mpourmpakis, D.G. Vlachos, ACS Catal. 2 (2012) 2496–2504.
[44] S. Wang, V. Vorotnikov, D.G. Vlachos, ACS Catal. 5 (2015) 104–112.
[45] J. Li, Z. Zhang, Z. Tian, et al., J. Mater. Chem. A 2 (2014) 16459–16466.